PROCEEDINGS OF SCIENCE

Two-loop calculation of the nucleon self-energy

Nils D. Conrad,[a,*] **Ashot Gasparyan**[a] **and Evgeny Epelbaum**[a]

[a] *Ruhr University Bochum, Faculty of Physics and Astronomy, Institute of Theoretical Physics II, D-44780 Bochum, Germany*

E-mail: nils.conrad@ruhr-uni-bochum.de, ashot.gasparyan@ruhr-uni-bochum.de, evgeny.epelbaum@ruhr-uni-bochum.de

The nucleon self-energy is calculated in SU(2) covariant chiral perturbation theory to study the pion mass dependence of the nucleon mass up to chiral order $O(q^6)$, i.e., including two-loop diagrams. Applying an algorithm proposed by Tarasov, the contributions of the diagrams are expressed by a small set of (scalar) master integrals. These master integrals are evaluated by means of the chiral expansion in d dimensions, using the strategy of regions to differentiate between the infrared singular and regular part. The extended on-mass-shell renormalization scheme is applied, making the renormalized expressions consistent with the power counting.

The 10th International Workshop on Chiral Dynamics - CD2021
15-19 November 2021
Online

[*] Speaker

PoS(CD2021)074

1. Introduction

Chiral perturbation theory (ChPT) is an effective field theory of quantum chromodynamics, which is the quantum field theory describing the strong force. The chiral Lagrangian is written in terms of the q/Λ expansion, where $q \sim M_\pi \sim |\vec{p}|$ is the soft scale of the order of the pion mass or the small external momentum and $\Lambda \sim 1$ GeV is the hard scale of the order of the not-included physics (see [1] for an extensive introduction into ChPT). For baryon chiral perturbation theory (BChPT), different renormalization methods are available to solve the power counting (PC) problem, for instance heavy baryon chiral perturbation theory (HBChPT) [2], the infrared scheme (IR) [3], and the extended-on-mass-shell renormalization (EOMS) [4, 5].

While having no PC violation per construction, HBChPT is not a manifestly Lorentz covariant theory and is known to have convergence problems. IR is covariant, but leads to the appearance of unphysical cuts. Finally, EOMS preserves not only Lorentz covariance, but also the analytic structure of the Green's functions. For a review of BChPT see [6].

This work focuses on the two-loop calculation of the nucleon mass up to chiral order six applying EOMS. An analysis of the chiral-order-five contributions was done in HBChPT [7], with the result that the M_π^5 contributions can be absorbed in the physical pion-nucleon coupling constant. A complete calculation up to chiral order six was already done in the IR scheme [8], working with the same Lagrangian and considering (nearly) the same diagrams as we do in the following.

This work is organized as follows: In section 2 we give some basics about the nucleon mass and self-energy in SU(2) chiral perturbation theory. In section 3 the reduction of the integrals is explained, while the solution of the remaining integrals is discussed in section 4. The renormalization is outlined in section 5. Finally, a summary and an outlook are given in section 6.

2. Nucleon mass in SU(2) chiral perturbation theory

In this section we introduce the SU(2) chiral Lagrangian and provide the basics for the calculation of the physical nucleon mass.

2.1 The SU(2) chiral Lagrangian

The SU(2) chiral Lagrangian $\mathcal{L} = \mathcal{L}_\pi^{(2)} + \mathcal{L}_\pi^{(4)} + \mathcal{L}_{\pi N}^{(1)} + \mathcal{L}_{\pi N}^{(2)} + \mathcal{L}_{\pi N}^{(3)} + \mathcal{L}_{\pi N}^{(4)} + \dots$ is built of a nucleon field Ψ and three pseudoscalar pion fields $\vec{\pi}$ and is listed up to order $O(q^4)$ in [9]. The lowest-order parts (including the free nucleon and pion parts) can be sketched as

$$\mathcal{L}_\pi^{(2)} = -\frac{1}{2}M^2\vec{\pi}\cdot\vec{\pi} + \frac{1}{2}\partial_\mu\vec{\pi}\cdot\partial^\mu\vec{\pi} + \frac{8\alpha-1}{8F^2}M^2\left(\vec{\pi}\cdot\vec{\pi}\right)^2 + \dots + O(\pi^6)\,, \tag{1}$$

$$\mathcal{L}_\pi^{(4)} = -\frac{(l_3+l_4)M^4}{F^2}\left(\vec{\pi}\cdot\vec{\pi}\right) + \dots + O(\pi^3)\,, \tag{2}$$

$$\mathcal{L}_{\pi N}^{(1)} = -\bar{\Psi}m\Psi + i\bar{\Psi}\not{\partial}\Psi + \frac{g_A}{2F}\bar{\Psi}\gamma_5\vec{\tau}\cdot\not{\partial}\vec{\pi}\Psi + \dots + O(\pi^5)\,. \tag{3}$$

Here, the pion mass M is of the order of the soft scale, and the nucleon mass m is of the order of the hard scale. The Lagrangian includes the low energy constants F, g_A, l_i as well as $c_i \in \mathcal{L}_{\pi N}^{(2)}$, $d_i \in \mathcal{L}_{\pi N}^{(3)}$, $e_i \in \mathcal{L}_{\pi N}^{(4)}$.[1]

[1] Where α is an arbitrary constant that cancels in the calculation of observables.

For quantum field theories, it is customary to calculate (physical) quantities in terms of Feynman diagrams, where each of these diagrams corresponds to a mathematical expression, determined by the Feynman rules (computed from the Lagrangian). The power counting of ChPT assigns a chiral order (in terms of the soft scale over the hard scale) to each of the diagrams and all integrals.

Because the order of a diagram increases by increasing the number of loops, no three-loop diagram has to be taken into account for a chiral-order-six calculation.

2.2 The nucleon mass and self-energy

The physical nucleon mass m_N is defined as the pole of the nucleon propagator via

$$\left[p^2 - (m + \Sigma(p, m))^2 + i\varepsilon\right]_{p^2 = m_N^2} = 0 \quad \Rightarrow \quad m_N = m + \Sigma(m_N, m), \tag{4}$$

where the self energy Σ is diagramatically defined as sum of all one-particle irreducible (1PI) diagrams, i.e., diagrams that cannot be divided into two by cutting one internal line.[2]

$-i\Sigma :=$ 

. (5)

The self energy consists of a (tree-level) contact part and a loop part $\Sigma = \Sigma_c + \Sigma_l$. The contact part can be easily calculated to be[3]

$$\Sigma_c = -4c_1 M^2 - 2\left(e_{115} + e_{116} + 8e_{38}\right) M^4 - \hat{g}_1 M^6 \,. \tag{6}$$

To simplify the calculations, we shift the nucleon mass in the self-energy $m \to m + \Sigma_c = \tilde{m}$, such that the physical nucleon mass is given by

$$m_N = \tilde{m} + \Sigma_l(m_N, \tilde{m}) \,, \tag{7}$$

where Σ_l now contains the contributions of the one-loop diagrams with the nucleon contact interactions included in the nucleon propagator (that is now a partly dressed propagator). All contributing one-loop and two-loop diagrams of Σ_l up to chiral order six are given in Fig. 1 and Fig. 2, where solid and dashed lines denote nucleons and pions respectively and the number in a vertex denotes the order of the Lagrangian it originates from.[4] For each diagram we denote the chiral order (according to the naive power counting) and the overall factor in terms of g_A and F.

3. Reduction to master integrals

The mathematical expressions of the diagrams are simplified and the (tensor) integrals are reduced to a small set of master integrals using the `Mathematica` program TARCER [10] based on Tarasov's

[2] All our expressions appear with Dirac spinors $u(p)$, so that with "$p = m_N$" we mean $p^2 = m_N^2$ and $\not{p} u(p) = m_N u(p)$.

[3] The order six term with constant $\hat{g}_1$ represents a linear combination of the contact terms from $\mathcal{L}_{\pi N}^{(6)}$.

[4] Note that Fig. 2d does not appear in [8] as its purely infrared-singular part vanishes up to higher order terms.

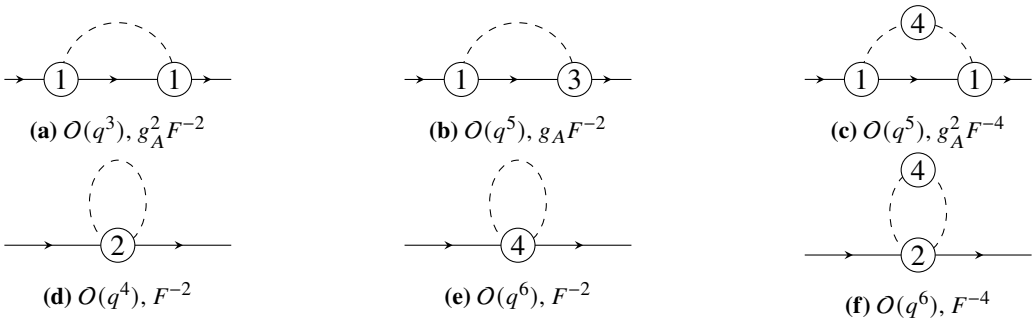

(a) $O(q^3)$, $g_A^2 F^{-2}$ **(b)** $O(q^5)$, $g_A F^{-2}$ **(c)** $O(q^5)$, $g_A^2 F^{-4}$

(d) $O(q^4)$, F^{-2} **(e)** $O(q^6)$, F^{-2} **(f)** $O(q^6)$, F^{-4}

Figure 1: One-loop diagrams contributing to the nucleon self-energy

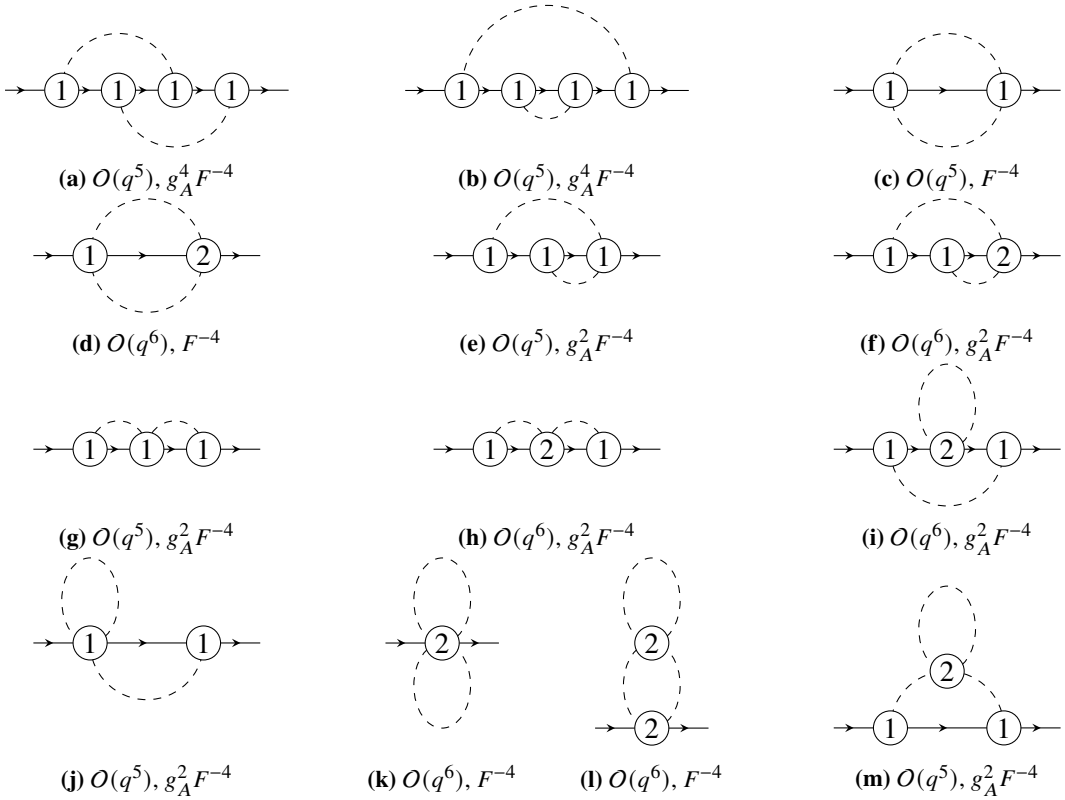

(a) $O(q^5)$, $g_A^4 F^{-4}$ **(b)** $O(q^5)$, $g_A^4 F^{-4}$ **(c)** $O(q^5)$, F^{-4}

(d) $O(q^6)$, F^{-4} **(e)** $O(q^5)$, $g_A^2 F^{-4}$ **(f)** $O(q^6)$, $g_A^2 F^{-4}$

(g) $O(q^5)$, $g_A^2 F^{-4}$ **(h)** $O(q^6)$, $g_A^2 F^{-4}$ **(i)** $O(q^6)$, $g_A^2 F^{-4}$

(j) $O(q^5)$, $g_A^2 F^{-4}$ **(k)** $O(q^6)$, F^{-4} **(l)** $O(q^6)$, F^{-4} **(m)** $O(q^5)$, $g_A^2 F^{-4}$

Figure 2: Two-loop diagrams contributing to the nucleon self-energy

reduction algorithm [11, 12]. Our set of master integrals consists of three single integrals $T_\pi^{(1)} = T_{M,0}^{(1)}(d;1,0)$, $T_N^{(1)} = T_{\tilde{m},0}^{(1)}(d;1,0)$ and $T_{\pi N}^{(1)} = T_{M,\tilde{m}}^{(1)}(d;1,1)$ and eight double integrals

$$
\begin{aligned}
T_{\mathrm{I}}^{(2)} &= T_{p,M,M,0,0,\tilde{m}}^{(2)}(d;1,1,0,0,1)\,, & T_{\mathrm{II}}^{(2)} &= T_{p,M,M,0,0,\tilde{m}}^{(2)}(d;2,1,0,0,1)\,,\\
T_{\mathrm{III}}^{(2)} &= T_{p,\tilde{m},\tilde{m},0,0,\tilde{m}}^{(2)}(d;1,1,0,0,1)\,, & T_{\mathrm{IV}}^{(2)} &= T_{p,M,M,0,0,\tilde{m}}^{(2)}(d;1,1,0,0,2)\,,\\
T_{\mathrm{V}}^{(2)} &= T_{p,M,0,0,\tilde{m},\tilde{m}}^{(2)}(d;1,0,0,1,1)\,, & T_{\mathrm{VI}}^{(2)} &= T_{p,M,M,\tilde{m},0,\tilde{m}}^{(2)}(d;1,1,1,0,1)\,,\\
T_{\mathrm{VII}}^{(2)} &= T_{p,M,0,\tilde{m},\tilde{m},\tilde{m}}^{(2)}(d;1,0,1,1,1)\,, & T_{\mathrm{VIII}}^{(2)} &= T_{p,M,M,\tilde{m},\tilde{m},\tilde{m}}^{(2)}(d;1,1,1,1,1)\,,
\end{aligned}
\tag{8}
$$

where we use the following integral definitions:

$$T^{(1)}_{p,m_1,m_2}(d;\alpha_1,\alpha_2) = \int \frac{\mathrm{d}^d l}{(2\pi)^d} \frac{1}{\left(l^2 - m_1^2 + i\varepsilon\right)^{\alpha_1} \left((l+p)^2 - m_2^2 + i\varepsilon\right)^{\alpha_2}}\,, \tag{9}$$

$$T^{(2)}_{p,\{m_k\}_{k=1}^5}(d;\beta_1,\beta_2,\beta_3,\beta_4,\beta_5) = \int \frac{\mathrm{d}^d l_1}{(2\pi)^d} \int \frac{\mathrm{d}^d l_2}{(2\pi)^d} \prod_{j=1}^{5} \frac{1}{\left(\tilde{l}_j^2 - m_j^2 + i\varepsilon\right)^{\beta_j}}\,, \tag{10}$$

$$\tilde{l}_1 = l_1,\ \tilde{l}_2 = l_2,\ \tilde{l}_3 = l_1 + p,\ \tilde{l}_4 = l_2 + p,\ \tilde{l}_5 = l_1 + l_2 + p\,. \tag{11}$$

The diagrammatic representations of these master integrals are given in Fig. 3 and Fig. 4.

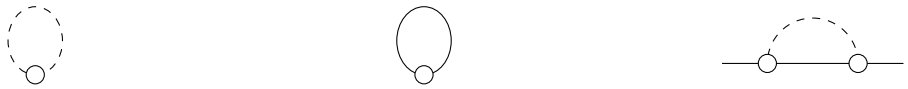

Figure 3: Diagrammatic representation of the single master integrals

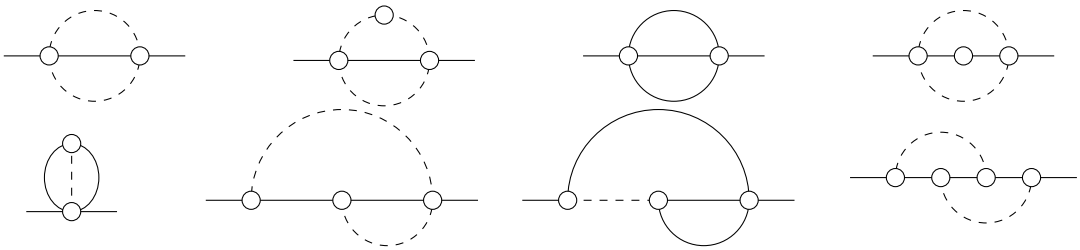

Figure 4: Diagrammatic representation of the double master integrals

For example, the reduced diagram Fig. 2e for $p^2 = \tilde{m}^2$ is given in terms of master integrals as

$$\begin{aligned}
-i\Sigma_e^{(2)} = &-\frac{ig_A^2\left((2d-3)\tilde{m}^2 - (d-2)M^2\right)}{2(3d-4)F^4\tilde{m}}(T_\pi^{(1)})^2 - \frac{3ig_A^2\tilde{m}}{F^4}(T_N^{(1)})^2 \\
&+\frac{ig_A^2\left(4(2d-3)\tilde{m}^2 - (d-2)M^2\right)}{2(3d-4)F^4\tilde{m}}T_N^{(1)}T_\pi^{(1)} - \frac{3ig_A^2\tilde{m}M^2}{F^4}T_N^{(1)}T_{\pi N}^{(1)} - \frac{3ig_A^2\tilde{m}M^2}{F^4}T_{\mathrm{V}}^{(2)} \\
&-\frac{ig_A^2\left(\left(8d^2-32d+30\right)\tilde{m}^4 + \left(-8d^2+33d-32\right)\tilde{m}^2M^2 - \left(d^2-5d+6\right)M^4\right)}{(d-2)(3d-4)F^4\tilde{m}}T_{\mathrm{I}}^{(2)} \\
&+\frac{4ig_A^2M^2\left(\tilde{m}^2 - M^2\right)\left((4d-6)\tilde{m}^2 + (d-2)M^2\right)}{(d-2)(3d-4)F^4\tilde{m}}T_{\mathrm{II}}^{(2)} - \frac{3ig_A^2\tilde{m}M^4}{F^4}T_{\mathrm{VI}}^{(2)}\,.
\end{aligned} \tag{12}$$

4. Solving the integrals with the strategy of regions

The single and double master integrals are solved using dimensional regularization. In the first step, the solutions are given as a chiral expansion in d-dimensional Minkowski space using the strategy of regions [13].

The idea is to expand the integrand in different regions, where the integration momenta are either of the order of the soft scale q or of the order of the hard scale. According to the strategy of regions, a Taylor series T_q in a small parameter q of an integral can be given by series of the

integrand in all possible regions. For example, a single integral over l would be expanded in two regions: one, where $l^2 \sim M^2 \sim q^2$, and one, where $l^2 \sim m^2 \gg q^2$:

$$T_q\left[\int f(l,q)\mathrm{d}l\right] = \int T_q\left[f(l,q)\right]_{l\sim q}\mathrm{d}l + \int T_q\left[f(l,q)\right]_{l\gg q}\mathrm{d}l = S + R\,. \tag{13}$$

The resulting parts are the infrared-singular part S, which is non-analytic in the soft scale q,[5] and the infrared-regular part, which is analytic in the soft scale q. In the case of a double integral there are four regions, such that

$$\begin{aligned} T_q\left[\int f(l_1,l_2,q)\mathrm{d}l_1\mathrm{d}l_2\right] &= \int T_q\left[f(l_1,l_2,q)\right]_{\substack{l_1\sim q\\ l_2\sim q}}\mathrm{d}l_1\mathrm{d}l_2 + \int T_q\left[f(l_1,l_2,q)\right]_{\substack{l_1\gg q\\ l_2\gg q}}\mathrm{d}l_1\mathrm{d}l_2 \\ &+ \left(\int T_q\left[f(l_1,l_2,q)\right]_{\substack{l_1\sim q\\ l_2\gg q}}\mathrm{d}l_1\mathrm{d}l_2 + \int T_q\left[f(l_1,l_2,q)\right]_{\substack{l_1\gg q\\ l_2\sim q}}\mathrm{d}l_1\mathrm{d}l_2\right) = S + R + M\,, \end{aligned} \tag{14}$$

where M is an additional mixed part (consisting out of two regions). The power-counting-breaking (PCB) terms stem from M and R, where at least one integration momentum is large.

For practical calculations, in regions with $l_i \sim q$, one can substitute $l_i^\nu \to M q_i^\nu$ (a dimensionless four-vector multiplied by the pion mass) and collect pion masses to get expressions like

$$\begin{aligned} &M^{d-4}\int\frac{\mathrm{d}^d q_1}{(2\pi)^d}\int\frac{\mathrm{d}^d l_2}{(2\pi)^d} \\ &\times\left\{\left[q_1^2-1\right]^2\left[l_2^2-M^2\right]\left[q_1^2M^2+2(l_2+p)\cdot q_1 M + l_2^2 + 2l_2\cdot p + p^2 - m^2\right]\right\}^{-1}, \end{aligned} \tag{15}$$

where in the next step one expands the integrand in M and p^2-m^2. The solutions for the remaining integrals are known (in terms of gamma and hypergeometric functions).

For technical and computational reasons, the master integrals were already expanded in the dimension $d-4$ before calculating the full expressions of the diagrams. For the expansion, the `Mathematica` package HypExp [14] was used. As an example, one obtains for the double master integral $T_{\mathrm{VI}}^{(2)}$ at leading chiral order (for simplicity we denote the masses as M and m):[6]

$$T_{\mathrm{VI}}^{(2),R} = -\frac{1}{128\pi^4(d-4)^2} + \frac{3}{256\pi^4(d-4)} + \frac{\pi^2-22}{1024\pi^4} + O(M^2,(d-4))\,, \tag{16}$$

$$T_{\mathrm{VI}}^{(2),S} = -\frac{M^2}{512\pi^2 m^2} + O(M^3,(d-4))\,, \tag{17}$$

$$T_{\mathrm{VI}}^{(2),M} = -\frac{M}{128\pi^3(d-4)m} - \frac{M\left(\ln\left(\frac{M}{m}\right)-1+\ln(2)\right)}{128\pi^3 m} + O(M^2,(d-4))\,. \tag{18}$$

Note that the naive PC predicts $T_{\mathrm{VI}}^{(2)}$ to be of chiral order two and that the purely infrared-regular part and the mixed part give PCB terms. Furthermore, the mixed part includes PCB terms, which are non-analytic in M^2.

Inserting these solutions of the master integrals, we computed all diagrams by means of the chiral expansion in different regions. For each diagram the purely infrared-singular part corresponds to the one from the reduced expressions from [8].[7]

[5] In the sense that q has powers in d, which is assumed to be a complex number.

[6] Where the renormalization scale is chosen as $\mu = (4\pi)^{-1/2}\exp((\gamma_E-1)/2)\,m$.

[7] Where we assume a typo in [8]: In $\delta m_{2(d)}$ in formula (108) an additional factor π^2 is missing for the dimension $n+4$ integrals.

5. Renormalization

The Lagrangian is given in terms of bare parameters $\tilde{m}^B$, M^B, F^B, g_A^B, c_i^B, ... Furthermore, the renormalized nucleon and pion fields appear with Z-factors Z_N and Z_π. We remind the reader that our goal is to get an expression for the physical nucleon mass from

$$m_N - \tilde{m}^B - \Sigma_l(m_N, \tilde{m}^B, \{\text{more bare parameters}\}) = 0\,. \tag{19}$$

5.1 Parameter Shifts

Following the EOMS renormalization from [15], we perform shifts

$$g_A^B \to g_A^B - 2(M^B)^2(2d_{16}^B - d_{18}^B)\,,\ (M^B)^2 \to (M^B)^2 - \frac{2l_3^B(M^B)^4}{(F^B)^2}\,,\ F^B \to F^B - \frac{l_4^B(M^B)^2}{F^B}\,, \tag{20}$$

thereby, effectively removing diagrams Fig. 1b, Fig. 1c and Fig. 1f (and the d_{16}, d_{18}, l_3 and l_4 dependence).

5.2 Corrections and the Z-factors

All bare parameters are given as the renormalized ones plus corrections like

$$\tilde{m}^B = \tilde{m}^R + \delta\tilde{m} = \tilde{m}^R + \hbar\delta\tilde{m}^{(1)} + \hbar^2\delta\tilde{m}^{(2)} + \dots\,. \tag{21}$$

The explicit (first order in $\hbar$) correction for the nucleon mass reads (following again [15])[8]

$$\begin{aligned}\delta\tilde{m}^{(1)} = {}& \frac{3i(g_A^R)^2\tilde{m}^R}{2(F^R)^2}T_N + \frac{3i(g_A^R)^2\tilde{m}^R(M^R)^2}{2(F^R)^2}T_{\pi N}^{\text{div+IRR}}(p^2 = m_N^2) \\ & - \frac{3c_2^R}{128\pi^2(F^R)^2}(M^R)^4 - \frac{i(M^R)^2(24c_1^R - 3(c_2^R + 4c_3^R))}{4(F^R)^2}T_\pi^{\text{div}},\end{aligned} \tag{22}$$

where only the divergent and infrared-regular parts (of chiral order zero) of the master integrals are taken. These corrections, as well as the corrections δM, δF, δg_A, δc_i, δe_i and δZ_N, produce additional terms in the Lagrangian (counterterms) that remove all divergent and power counting breaking (PCB) terms of the diagrams.

The Z-factors $\Psi^B = \sqrt{Z_N}\Psi^R = \sqrt{1+\delta Z_N}\Psi^R$ and $\pi_a^B = \sqrt{Z_\pi}\pi_a^R = \sqrt{1+\delta Z_\pi}\pi_a^R$ give the following additional counterterms stemming from the free and the contact part of the Lagrangian:

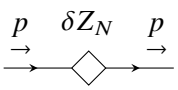

$$\hat{=}\ i\delta Z_N\left(\not{p} - \tilde{m}^R\right),$$

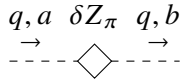

$$\hat{=}\ i\delta Z_\pi\left(q^2 - \left(M^R\right)^2\right)\delta_{ab}. \tag{23}$$

In diagrams, these terms cancel one of the propagators and effectively give a factor $-\delta Z_N$ or $-\delta Z_\pi$ per nucleon or pion line. In addition, each vertex with one incoming and one outgoing nucleon

[8] Note that we work with the shifted mass, where $\tilde{m} = m^R + \Sigma_c^R + \delta m + \delta\Sigma_c$. The terms $4c_1^R(M^R)^2$ and $4c_1^R\delta(M^2)$ are included in the contact self-energy (also including $4\delta c_1(M^R)^2$ and higher chiral order terms).

line gives a contribution δZ_N or $\delta Z_\pi/2$ per pion propagator. Therefore, the correction to the pion Z-factor does not contribute to our calculation, while the nucleon Z-factor in total contributes as factor δZ_N times the one-loop diagrams.

The diagrams involving counterterms are given in Fig. 5, Fig. 6 and Fig. 7, and in general contribute at different overall factors in g_A and F.

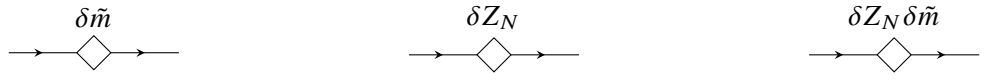

(a) $F^{-2}, g_A^2 F^{-2}$ **(b)** $g_A^4 F^{-4}$ **(c)** $g_A^2 F^{-4}, g_A^4 F^{-4}$

Figure 5: Tree-level counterterm diagrams contributing to the nucleon self-energy

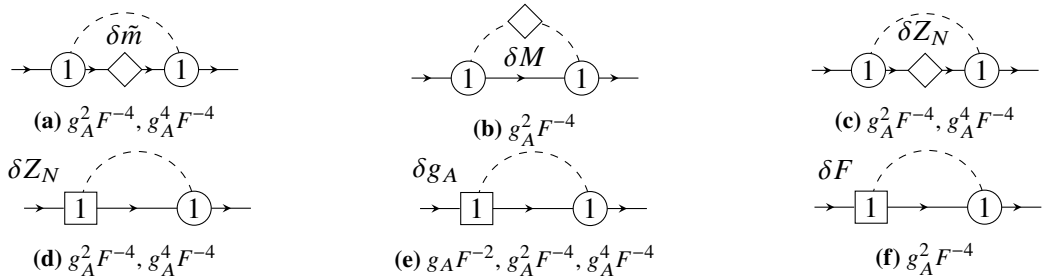

(a) $g_A^2 F^{-4}, g_A^4 F^{-4}$ **(b)** $g_A^2 F^{-4}$ **(c)** $g_A^2 F^{-4}, g_A^4 F^{-4}$

(d) $g_A^2 F^{-4}, g_A^4 F^{-4}$ **(e)** $g_A F^{-2}, g_A^2 F^{-4}, g_A^4 F^{-4}$ **(f)** $g_A^2 F^{-4}$

Figure 6: One-loop counterterm diagrams corresponding to Fig. 1a

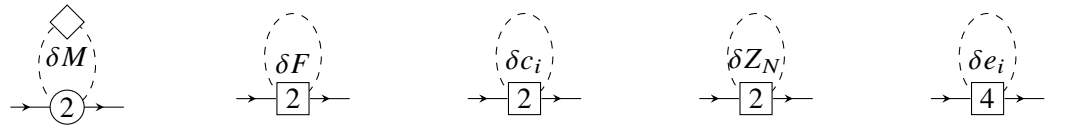

(a) F^{-4} **(b)** F^{-4} **(c)** $F^{-4}, g_A^2 F^{-4}, g_A^4 F^{-4}$ **(d)** $g_A^2 F^{-4}$ **(e)** $F^{-4}, g_A^2 F^{-4}, g_A^4 F^{-4}$

Figure 7: One-loop counterterm diagrams corresponding to Fig. 1d and Fig. 1e

5.3 Renormalized result in terms of the chiral expansion

As a first step, we use $\tilde{m}^B = m_N + \delta\tilde{m}$, which yields for Eq. (19): $\Sigma_l + \delta\tilde{m} = 0$. This choice allows an on-shell calculation of all diagrams due to $(\tilde{m}^R)^2 = p^2$.

Adding the expressions for the counterterm diagrams to the expressions for Fig. 1 and Fig. 2, the divergences and all analytic PCB terms from the purely infrared-regular parts as well as all non-analytic PCB terms stemming from the mixed parts are removed. The only PCB terms from the one-loop diagrams left are from Fig. 1e and they are proportional to $e_i M^6$ and added to $\delta m_N^{(1)}$. The remaining analytic PCB parts from the two-loop diagrams are included in $\delta m_N^{(2)}$. The renormalized self-energy is given by (with all constants being renormalized ones)

$$\Sigma_l + \delta\tilde{m} = \frac{1}{F^2} t_{0,2} + \frac{g_A^2}{F^2} t_{2,2} + \frac{1}{F^4} t_{0,4} + \frac{g_A^2}{F^4} t_{2,4} + \frac{g_A^4}{F^4} t_{4,4}\,. \tag{24}$$

$$\frac{1}{F^2}t_{0,2} = \frac{3c_1M^4}{4\pi^2F^2}\ln\left(\frac{M}{m_N}\right) - \frac{3c_2M^4}{32\pi^2F^2}\ln\left(\frac{M}{m_N}\right) - \frac{3c_3M^4}{8\pi^2F^2}\ln\left(\frac{M}{m_N}\right) + \frac{M^6}{32\pi^2F^2}\left\{\text{sum of } e_i - 12\,(\text{another sum of } e_i)\ln\left(\frac{M}{m_N}\right)\right\} \tag{25}$$

$$\frac{g_A^2}{F^2}t_{2,2} = -\frac{3g_A^2M^3}{32\pi F^2} + \frac{3g_A^2M^4}{32\pi^2F^2m_N}\left(1 - \ln\left(\frac{M}{m_N}\right)\right) + \frac{3g_A^2M^5}{256\pi F^2m_N^2} - \frac{g_A^2M^6}{128\pi^2F^2m_N^3} \tag{26}$$

$$\frac{1}{F^4}t_{0,4} = -\frac{M^6}{12288\pi^4F^4}\left\{-144(2c_1-c_3)\ln\left(\frac{M}{m_N}\right) - 144(6c_1-c_2-4c_3)\ln^2\left(\frac{M}{m_N}\right) - 24\left(6+\pi^2\right)c_1 + 18c_2 + 3\pi^2c_2 + 72c_3 + 12\pi^2c_3 + 32c_4 + 60\pi^2c_4 - \frac{30}{m_N}\right\} \tag{27}$$

$$\frac{g_A^2}{F^4}t_{2,4} = -\frac{9g_A^2M^5\ln\left(\frac{M}{m_N}\right)}{1024\pi^3F^4} - \frac{g_A^2M^6}{64\pi^2F^4m_N} + \frac{9g_A^2M^6}{256\pi^4F^4m_N} - \frac{3g_A^2M^6\ln^2\left(\frac{M}{m_N}\right)}{256\pi^4F^4m_N} - \frac{5g_A^2M^6\ln\left(\frac{M}{m_N}\right)}{1024\pi^4F^4m_N} + \frac{g_A^2M^6}{18432\pi^4F^4}\left\{3348c_1 - 438c_2 - 398c_3 + 2140c_4 + 3\pi^2(42c_1+5c_2+119c_3-226c_4) + 486(8c_1-c_2-4c_3)\ln^2\left(\frac{M}{m_N}\right)\right\} \tag{28}$$

$$\frac{g_A^4}{F^4}t_{4,4} = -\frac{g_A^4M^5}{128\pi^3F^4} + \frac{21g_A^4M^5\ln\left(\frac{M}{m_N}\right)}{1024\pi^3F^4} - \frac{g_A^4M^6\left(239\left(8+3\pi^2\right) + 864\ln\left(\frac{M}{m_N}\right) + 2592\ln^2\left(\frac{M}{m_N}\right)\right)}{98304\pi^4F^4m_N} \tag{29}$$

As a next step, we use $\tilde{m}^B = m_0 + \Sigma_c^R + \delta\tilde{m}$, which yields for Eq. (19): $m_N = m_0 + \Sigma_c^R + \delta\tilde{m} + \Sigma_l = 0$. Expressing the external momentum in the diagrams as

$$\sqrt{p^2} = m_N = m_0 + \Sigma_c^R - \frac{3g_A^2M^3}{32\pi F^2} + O(M^4)\,, \tag{30}$$

we get additional terms from $m_N - \tilde{m}^R \sim O(M^3)$. Using the same corrections as before, additional terms from the purely infrared-singular part that are non-analytic in M^2 only appear two chiral orders higher than the order of the diagrams. Diagrams contributing additional non-analytic terms are the one-loop diagram Fig. 1a and the tree-level counterterm diagram Fig. 5b, the expression of which includes a factor $\not{p} - \tilde{m}^R$ (see Eq. (23)).

6. Summary and outlook

We have successfully reduced the mathematical expressions of all two-loop diagrams contributing to the nucleon mass up to and including chiral order six and calculated all diagrams by means of the chiral expansion using the strategy of regions. We were able to show that all power-counting-breaking terms (as well as all divergent terms) can be removed using the EOMS renormalization. We also presented the renormalized self-energy.

In the next step, we will analyze the additional terms from the off-shell case in more detail. The final expanded result should then be compared to the existing HB and the IR results.

Clearly, our final goal is to calculate the nucleon self-energy without relying on the chiral (i.e. $1/m$) expansions. Because products of single integrals appear in the reduced expressions of the two-loop diagrams, we need the full solution for the single pion-nucleon integral up to and including the linear order in $d-4$. For the double master integrals a separation of analytic and finite parts has to be computed and the finite parts have to be calculated numerically. This work is in progress.

Acknowledgments

We would like to thank Jambul Gegelia for discussions and help with solving integrals. This work was supported by DFG and NSFC through funds provided to the Sino-German CRC 110 "Symmetries and the Emergence of Structure in QCD" (NSFC Grant No. 11621131001, DFG Project-ID 196253076-TRR 110), by DFG (Grant No. 426661267), by ERC AdG Nuclear Theory (Grant No. 885150) and by the EU Horizon 2020 research and innovation programme (STRONG-2020, grant-agreement No. 824093).

References

[1] S. Scherer and M. R. Schindler, Lect. Notes Phys. **830** (2012), pp.1-338.

[2] E. E. Jenkins and A. V. Manohar, Phys. Lett. B **255** (1991), 558-562.

[3] T. Becher and H. Leutwyler, Eur. Phys. J. C **9** (1999), 643-671 [arXiv:hep-ph/9901384 [hep-ph]].

[4] J. Gegelia and G. Japaridze, Phys. Rev. D **60** (1999), 114038 [arXiv:hep-ph/9908377 [hep-ph]].

[5] T. Fuchs, J. Gegelia, G. Japaridze and S. Scherer, Phys. Rev. D **68** (2003), 056005 [arXiv:hep-ph/0302117 [hep-ph]].

[6] V. Bernard, Prog. Part. Nucl. Phys. **60** (2008), 82-160 [arXiv:0706.0312 [hep-ph]].

[7] J. A. McGovern and M. C. Birse, Phys. Lett. B **446** (1999), 300-305 [arXiv:hep-ph/9807384 [hep-ph]].

[8] M. R. Schindler, D. Djukanovic, J. Gegelia and S. Scherer, Nucl. Phys. A **803** (2008), 68-114 [erratum: Nucl. Phys. A **1010** (2021), 122175] [arXiv:0707.4296 [hep-ph]].

[9] N. Fettes, U.-G. Meißner, M. Mojzis and S. Steininger, Annals Phys. **283** (2000), 273-302 [erratum: Annals Phys. **288** (2001), 249-250] [arXiv:hep-ph/0001308 [hep-ph]].

[10] R. Mertig and R. Scharf, Comput. Phys. Commun. **111** (1998), 265-273 [arXiv:hep-ph/9801383 [hep-ph]].

[11] O. V. Tarasov, Phys. Rev. D **54** (1996), 6479-6490 [arXiv:hep-th/9606018 [hep-th]].

[12] O. V. Tarasov, Nucl. Phys. B **502** (1997), 455-482 [arXiv:hep-ph/9703319 [hep-ph]].

[13] M. Beneke and V. A. Smirnov, Nucl. Phys. B **522** (1998), 321-344 [arXiv:hep-ph/9711391 [hep-ph]].

[14] T. Huber and D. Maitre, Comput. Phys. Commun. **175** (2006), 122-144 doi:10.1016/j.cpc.2006.01.007 [arXiv:hep-ph/0507094 [hep-ph]].

[15] D. Siemens, V. Bernard, E. Epelbaum, A. Gasparyan, H. Krebs and U.-G. Meißner, Phys. Rev. C **94** (2016) no.1, 014620 [arXiv:1602.02640 [nucl-th]].